AGU PUBLICATIONS

Geochemistry, Geophysics, Geosystems

RESEARCH ARTICLE
10.1002/2015GC006119

Key Points:
- Modeled fluxes are <0.1% of global atmospheric CH_4 budget
- About 70% of produced CH_4 from dissociation remains trapped in the sediments
- The amount of hydrate on continental slopes and potential fluxes depend strongly on past sea level

Supporting Information:
- Supporting Information S1

Correspondence to:
C. Stranne,
christian.stranne@geo.su.se

Citation:
Stranne, C., M. O'Regan, G. R. Dickens, P. Crill, C. Miller, P. Preto, and M. Jakobsson (2016), Dynamic simulations of potential methane release from East Siberian continental slope sediments, *Geochem. Geophys. Geosyst.*, *17*, 872–886, doi:10.1002/2015GC006119.

Received 29 SEP 2015
Accepted 12 FEB 2016
Accepted article online 17 FEB 2016
Published online 12 MAR 2016

Dynamic simulations of potential methane release from East Siberian continental slope sediments

C. Stranne[1,2,3], M. O'Regan[1,2], G. R. Dickens[1,4], P. Crill[1,2], C. Miller[4], P. Preto[1,2], and M. Jakobsson[1,2]

[1]Department of Geological Sciences, Stockholm University, Stockholm, Sweden, [2]Bolin Centre for Climate Research, Stockholm University, Stockholm, Sweden, [3]Center for Coastal & Ocean Mapping/Joint Hydrographic Center, Durham, New Hampshire, USA, [4]Department of Earth Science, Rice University, Houston, Texas, USA

Abstract Sediments deposited along continental margins of the Arctic Ocean presumably host large amounts of methane (CH_4) in gas hydrates. Here we apply numerical simulations to assess the potential of gas hydrate dissociation and methane release from the East Siberian slope over the next 100 years. Simulations are based on a hypothesized bottom water warming of 3°C, and an assumed starting distribution of gas hydrate. The simulation results show that gas hydrate dissociation in these sediments is relatively slow, and that CH_4 fluxes toward the seafloor are limited by low sediment permeability. The latter is true even when sediment fractures are permitted to form in response to overpressure in pore space. With an initial gas hydrate distribution dictated by present-day pressure and temperature conditions, nominally 0.35 Gt of CH_4 are released from the East Siberian slope during the first 100 years of the simulation. However, this CH_4 discharge becomes significantly smaller (~0.05 Gt) if glacial sea level changes in the Arctic Ocean are considered. This is because a lower sea level during the last glacial maximum (LGM) must result in depleted gas hydrate abundance within the most sensitive region of the modern gas hydrate stability zone. Even if all released CH_4 reached the atmosphere, the amount coming from East Siberian slopes would be trivial compared to present-day atmospheric CH_4 inputs from other sources.

1. Introduction

Continental slopes host large quantities of methane (CH_4). This CH_4 exists in sediment pore space as gas hydrates, free gas bubbles, and dissolved gas, the first of these being an ice-like solid [*Hester and Brewer*, 2009]. Global estimates for the mass of carbon within subseafloor CH_4 remain somewhat unconstrained; a reasonable estimate for the present-day gas hydrate portion lies between 1000 and 5000 metric gigatons (Gt) of carbon [*Beaudoin et al.*, 2014]. This submarine CH_4 reservoir is dynamic, with continuous inputs and outputs of carbon over time; it is also sensitive to variations in ocean temperature and pressure (sea level) [*G. R. Dickens*, 2001a]. Consequently, CH_4 release from ocean sediments may be an important component of carbon cycling and climate [*Dickens*, 2003; *Archer*, 2007, 2015; *Lunt et al.*, 2011]. More specifically, warming of ocean bottom water should lead to greater CH_4 fluxes from the seafloor, which would impact ocean chemistry, atmospheric greenhouse gas loads, or both.

The Arctic Ocean is "ground zero" for discussions on potential thermal release of CH_4 from the seafloor [*Paull et al.*, 1991; *Archer*, 2007; *Elliott et al.*, 2010, 2011; *Isaksen et al.*, 2011; *Ferré et al.*, 2012; *Giustiniani et al.*, 2013; *Marín-Moreno et al.*, 2013; *Thatcher et al.*, 2013; *Phrampus et al.*, 2014]. As noted in these papers, three factors contribute to this focused attention: (1) vast quantities of CH_4 (670–1200 Gt) may exist as gas hydrates in sediments along continental margins of the Arctic Ocean [*Kvenvolden*, 1989; *Biastoch et al.*, 2011]; (2) relatively cold bottom water temperatures place the upper limit of the gas hydrate stability zone (GHSZ) at shallow water depths (~300 m) along continental slopes [*Reagan and Moridis*, 2008; *Ruppel*, 2011]; and (3) warming may happen in the Arctic significantly faster over the next 100 years than elsewhere, perhaps twice the global average [*Serreze and Barry*, 2011].

A recent United Nations (UN) report on gas hydrates [*Beaudoin et al.*, 2014] poses several questions that remain unanswered. Among these are two basic ones: (1) how much gas hydrate will dissociate in marine sediment from projected ocean warming? and (2) how much methane released from destabilized gas hydrates will be transferred to the atmosphere? Interestingly, the UN report, and indeed most research

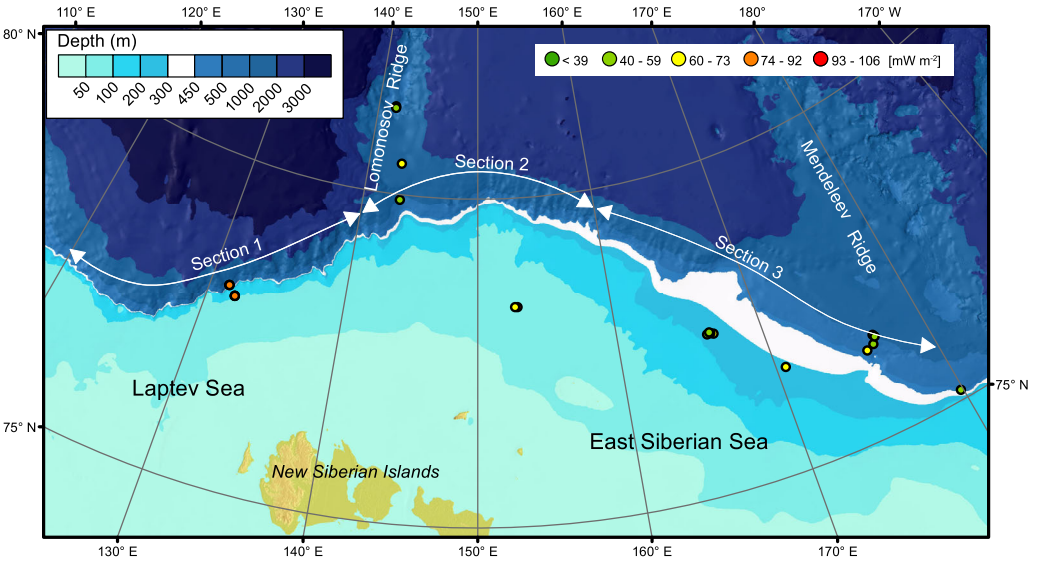

Figure 1. Map showing the study area with the horizontal model domain (white area). Colored dots indicate locations for heat flow observations. The bathymetry is taken from the IBCAO bathymetry data set [*Jakobsson et al.*, 2012].

literature on gas hydrates, circumvents a related question: how much free CH_4 gas produced by hydrate dissociation will remain trapped within the sediments? The answers lie mostly with models that capture the complexities of multiphase flow within marine sediments. It is not a simple case that gas hydrate dissociation directly leads to enhanced seafloor CH_4 fluxes; there are, for example, the rise in pore pressures with gas production (with consequences for dissociation rates and possible fracture formation), and the changes in relative permeability as solid hydrates are replaced by gas. *Reagan and Moridis* [2008] showed, through numerical modeling, that significant portions of CH_4 gas formed from gas hydrate dissociation can remain within sediments on a centennial time scale.

Here we use a numerical model to improve our understanding of how CH_4-bearing phases might evolve in continental slope sediments of the East Siberian Sea, a large and underexplored region of the Arctic Ocean (Figure 1). We begin with an important caveat: while the problem is great, the assumptions are greater. We assume a range of initial gas hydrate distributions in the sediment, and a linear rise in ocean bottom water temperatures of 3°C over 100 years, after which the bottom water temperatures remain constant for the rest of the simulation. This Arctic Ocean warming is intentionally set higher than in other studies (<2°C) [*Biastoch et al.*, 2011; *Kretschmer et al.*, 2015] so that we do not underestimate potential warming-induced hydrate dissociation. An offline approach to handle formation of sediment fractures and transport of CH_4 gas through such fractures was developed because these processes are not considered in the present numerical model.

2. Study Area: East Siberian Slope

Gas hydrates definitely exist along continental slopes of the Arctic Ocean in several locations including the Canadian Beaufort Sea [*Weaver and Stewart*, 1982], Alaskan continental slope [*Grantz and Dinter*, 1980; *Kvenvolden and Grantz*, 1990], and the West Spitsbergen margin [*Posewang and Mienert*, 1999]. On the East Siberian margin, significant CH_4 escape from the continental shelf has been documented. [*Shakhova et al.*, 2015]. Likely, gas hydrates also occur along the adjacent continental slope [*Kvenvolden and Grantz*, 1990; *Max and Lowrie*, 1993], with CH_4 produced from either microbial degradation of organic material delivered from the shelf [*Archer*, 2015], or thermogenic degradation of deeply buried organic-rich sediments [*Khain et al.*, 2009; *Drachev*, 2011]. So far, though, a lack of seismic and borehole data from this ice-covered area precludes firm ground truthing of gas hydrate along the slopes of East Siberia.

Similar to the West Spitsbergen margin [*Westbrook et al.*, 2009], inflowing Atlantic water directly influences the East Siberian continental slope. An eastward propagating warmth of water along the slope has been documented for the Nansen Basin [*Polyakov et al.*, 2007]. Assuming this warming continues over the coming decades and centuries, stability conditions affecting gas hydrate distribution will be altered. Due to this

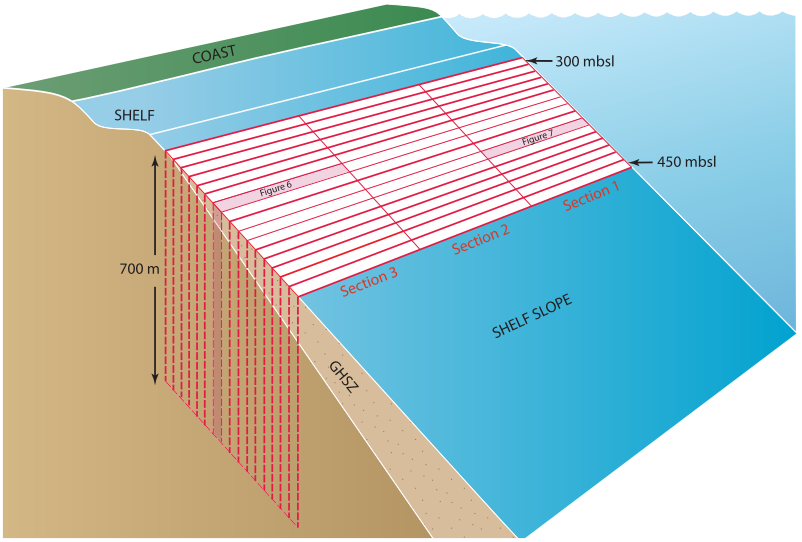

Figure 2. A schematic cartoon showing the model setup with 48 grid cells in the horizontal model domain. Each grid cell includes a column model extending 700 mbsf, with individual initial and boundary conditions based on section and seafloor depth. Note that the large variability in horizontal area between the grid cells (Figure 3 and supporting information Table S2) is not reflected in this figure.

probable future increase in bottom water temperature, and due to its vast areal extent, the East Siberian margin seems a critical area in which to constrain CH_4 emissions from the seabed.

In the summer of 2014, a major international research program, the Swedish-Russian-United States investigation of Climate, Cryosphere and Carbon interaction (SWERUS-C3), investigated the East Siberian margin using the Swedish icebreaker *Oden*. One key goal of this project was to constrain the amount and fluxes of CH_4 within this generally inaccessible and largely unexplored region. Notably, the second expedition was devoted to generating remote geophysical information regarding the seafloor, and to collecting physical, chemical, and geological data in piston cores along multiple transects across the continental slope. The amount, distribution, and fluxes of CH_4 within the large area are the focus of current research efforts. The present modeling study was designed ahead of time with two aims in mind: (1) to assess the sensitivity of gas hydrates in sediment along the upper continental slope of East Siberia upon an increase in temperature, but (2) to make the effort broadly applicable to any continental slope where dominantly fine-grained, terrigenous sediments form sequences with relatively low permeability.

2.1. Modeling Approach

Gas hydrates can occur within sediment across a depth interval commonly referred to as the GHSZ (Figure 2). The base of the GHSZ marks the depth where pressures and temperatures along the geotherm intersect with those on an appropriate three-phase (gas hydrate-free gas-dissolved gas) equilibrium curve. Because the equilibrium curve depends on pressure, temperature, water activity (~salinity), and gas composition [*Handa*, 1990; *Dickens and Quinby-Hunt*, 1997], vertical dimensions of the GHSZ vary geographically, both along and across continental margins [*G. R. Dickens*, 2001b]. Near sites of high upward fluid advection (e.g., seafloor seeps), in situ temperature, and salinity profiles can be complex [*Milkov*, 2004; *Ruppel et al*., 2005], and gas may include significant quantities of ethane, propane, and butane [*Collett et al*., 1988; *Sassen et al*., 2001]. Presumably, however, at many seafloor sites with gas hydrate, in situ pressure approximates hydrostatic conditions, in situ temperature follows the regional geothermal gradient, in situ water activity is close to or slightly less than that of seawater, and the gas principally consists of CH_4. This inference is borne-out from scientific drilling [*Paull and Matsumoto*, 2000; *Tréhu et al*., 2004; *Bahk et al*., 2013]. Consequently, across most continental margins, the GHSZ exists as a lens that starts at some shallow water depth determined by bottom water temperature, and generally expands down the slope because of increasing water depth [e.g., *G. R. Dickens*, 2001b; *Ruppel*, 2011].

To tackle the problem of potential seafloor CH_4 release from dissociation of gas hydrate across a region, four broad aspects need consideration: (1) the current extent of the GHSZ, (2) the distribution of CH_4 within

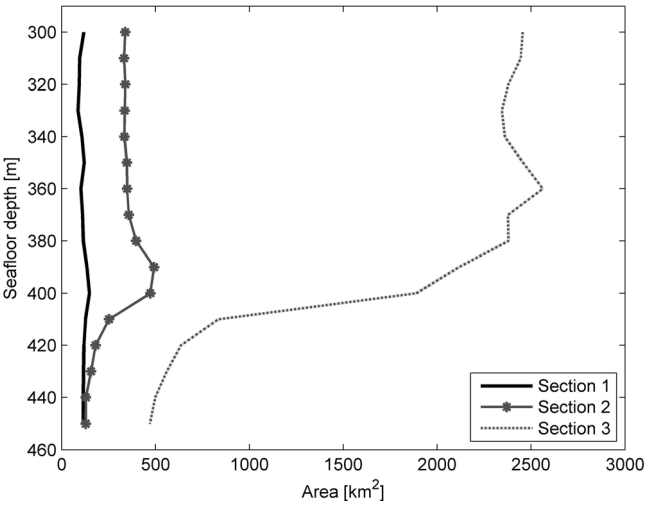

Figure 3. Area distribution for the three sections calculated from the IBCAO bathymetry data set [*Jakobsson et al*., 2012], see supporting information Table S1 for details.

the GHSZ, (3) how the GHSZ should change over time in response to a seafloor temperature perturbation, and (4) how sediment CH_4 content would evolve in the perturbed system. Given current unknowns for the East Siberian margin, but overall objectives of this work, our approach here was to address the latter two facets (3 and 4) based on assumptions regarding the former two facets (1 and 2). We therefore consider a plausible range of gas hydrate saturation values along slopes of the East Siberian margin. However, the extent of the GHSZ depends partly on gas hydrate saturation. This is because between differences in the thermal conductivity of "seawater" and gas hydrate within pore space (as elaborated upon in section 2.3 below).

The TOUGH+Hydrate (T+H) model [*Moridis*, 2014] was used to address how gas hydrate within slope sediments would respond to seafloor warming. This model simulates multiphase flow in hydrate-bearing geologic media. It includes coupled mass and energy transport and the full phase behavior of water, methane, solid hydrate, ice, and inhibitor species (in this case NaCl). The model has been examined and refined with results from laboratory experiments [*Liang-Guang Tang*, 2006] and in field studies [*Moridis et al*., 2005].

The T+H model has been used previously to simulate the response of gas hydrate deposits in the Arctic Ocean to ocean warming. *Reagan and Moridis* [2008] investigated hydrate dissociation and CH_4 transport to the ocean using a generic 1-D Arctic shelf slope case (representing a shallow-cold deposit) with homogeneous sediment physical properties. The T+H model has also been set up for specific locations within the Arctic Ocean [*Reagan and Moridis*, 2009; *Marín-Moreno et al*., 2013; *Thatcher et al*., 2013]. *Reagan and Moridis* [2009] applied a parallel version of the T+H code to perform 2-D simulations of a 5000 m shelf slope transect west of Spitsbergen. For practical reasons, given the large horizontal length scales in our present study, and because the error in the 1-D approximation by comparison with 2-D is very small for typical shelf slope angles in the present study area [*Reagan et al*., 2011], we use the 1-D model code in the present study.

We apply the T+H model to the upper slope along the East Siberian margin (Figure 1) by setting up a grid of 1-D column models, each with individual boundary conditions (seafloor temperature, pressure, and geothermal heat flow). The region extends from the Laptev Sea to the East Siberian Sea, or between 120°E and 180°E longitude; it covers water depths from 300 to 450 m below current sea level. This $\sim 3.6 \cdot \times 10^7$ km^2 area should represent the "feather edge" of the regional GHSZ [*Ruppel*, 2011], the part of the slope most sensitive to seafloor temperature perturbations. It is not relevant to extend the shelf slope transects further down slope because, although gas is produced at the base of the GHSZ in the model, the overlying hydrates act as an impermeable lid effectively preventing vertical migration of free gas, and in situ pressure never approaches the threshold for fracture formation (as elaborated upon in section 2.4 below).

The horizontal component of the model domain was divided into a grid that consists of three longitudinal sections and 16 depth intervals (Figure 2). These 48 seafloor grid cells have different spatial parameters, seafloor temperature and pressure, and geothermal heat flow (Figure 3 and supporting information Table S1). Our approach is somewhat similar to that in the study by *Marín-Moreno et al*. [2013], where the T+H model was set up for one section of the upper slope west of Svalbard. In their work, six grid cells were placed between 400 and 800 meters below sea level (mbsl).

The vertical component of the model domain extends to 700 m below the seafloor (mbsf) with 1280 grid cells increasing exponentially in size from 0.02 m at the seafloor to 2.7 m at the lower boundary. In previous T+H model studies, vertically homogeneous sediment physical properties were assumed for the whole sediment

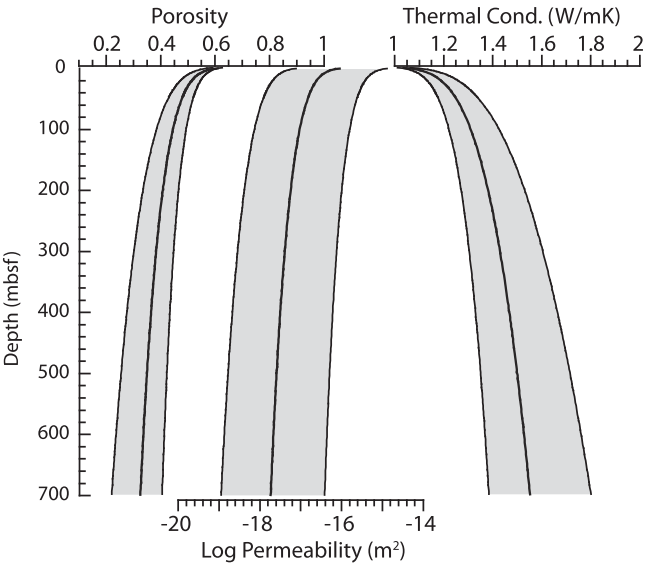

Figure 4. Sediment physical properties model with shaded 95% confidence intervals.

column [*Reagan and Moridis*, 2008, 2009; *Reagan et al*., 2011; *Thatcher et al*., 2013] or within two layers [*Marín-Moreno et al*., 2013]. In our model setup, sediment physical properties (permeability, porosity, and wet/dry thermal conductivity) depend on depth. The loss of porosity with greater depth and sediment burial is important, because it results in a nonlinear increase in thermal conductivity [Stranne and Oregan, 2015] and a nonlinear decrease in permeability (Figure 4**)**. The sediment physical properties used are based on laboratory testing of sediments from the Lomonosov Ridge (supporting information). The vertical change in these properties is represented in each model column by 500 regions starting at a grid size of 0.02 m and increasing exponentially to 8.4 m at the lower boundary. Model parameters and boundary conditions are listed in Table 1.

This study is the first to simulate the predicted behavior of CH_4 along the East Siberian margin with a state-of-the-art multiphase sediment flow model. More importantly, though, it differs in detail from similar dynamical simulation efforts on other margins in that: (1) we set up an array of 48 column models to take into account regional variations in seafloor temperature and geothermal heat flow, (2) we use detailed bathymetry to assess the integrated CH_4 gas escape over the model domain, (3) we use a rigorous and regionally applicable sediment physical property model, and (4) we allow for sediment physical properties to vary with depth.

2.2. Model Input

Seafloor temperature and pressure conditions were extracted from the World Ocean Atlas 2013 (WOA13) [*Locarnini et al*., 2013]. This was done through a nearest neighbor interpolation of WOA13 data to each IBCAO bathymetry grid cell [*Jakobsson et al*., 2012] falling within a horizontal grid cell used in this study. The mean seafloor temperature was then calculated for each model seafloor grid cell and used as a boundary condition for the individual columns (supporting information Table S1).

The average heat flow for each horizontal grid cell was obtained from published measurements of the East Siberian continental slope, southern Lomonosov Ridge, and the Laptev Sea, which are available in the International Heat Flow Committee (IHFC)'s Global Heat Flow Database [*Pollack et al*., 1993; *Gosnold and Panda*, 2002]. These data were augmented by measurements taken during the 2014 SWERUS-C3 expedition (supporting information). The combined data allowed us to approximate large-scale regional heat flow variations with average values of 0.087 Wm^{-2} between 120°E and 140°E, 0.068 Wm^{-2} between 140°E and 160°E, and 0.055 Wm^{-2} between 160°E and 180°E.

Table 1. Model Parameters

Parameter	Value
Initial/boundary salt mass fraction	0.035
Gas composition	100% CH_4
Hydrate saturation, H_s	3%
Permeability	See section 2.2
Porosity	See section 2.2
Wet/dry thermal conductivity	See section 2.2
Composite thermal conductivity	*Moridis* [2014]
Capillary pressure model	*Van Genuchten* [1980] with parameters taken from *Thatcher et al.* [2013]
Relative permeability model	Modified Stone model [*Moridis*, 2014], with parameters taken from *Thatcher et al.* [2013]
Sediment density	2700 kg m^{-3}
Geothermal heat flow	See section 2.2

The above parameters permit calculation of an initial GHSZ along the upper continental slope north of Siberia (assuming that pore water has a salinity similar to standard seawater and that

Table 2. Model Simulations

Simulation Case	Description
A	Baseline (H_s = 3% within the GHSZ)
B	Partly hydrate reservoir depletion from LGM sea levels
C1	H_s = 5% within the GHSZ
C2	H_s = 1% within the GHSZ
D1	High porosity (see supporting information)
D2	Low porosity (see supporting information)
E1	20% increased geothermal heat flow (see supporting information)
E2	20% decreased geothermal heat flow (see supporting information)

gas hydrates contain CH_4 as the only gas). Within this starting potential volume [*G. R. Dickens*, 2001b], we impose several possible initial gas hydrate distributions. For each of these distributions (hereafter referred to as cases), we assume that the upper 6 m of the sediment column lacks gas hydrate. This is because shallow sediment above gas hydrate systems generally has a depth interval with SO_4^{2-} and no CH_4 (the oft-called sulfate reduction zone, SRZ), as well as a depth interval with CH_4 but at concentrations less than that to form gas hydrate [*Bhatnagar et al*., 2011]. The chosen value is taken from baseline cases (5–7 m) in previous works [*Wallmann et al*., 2012; *Biastoch et al*., 2011; *Thatcher et al*., 2013]. It is worth noting that the SRZ alone typically exceeds 6 m over seafloor areas above gas hydrate systems [e.g., *Paull and Matsumoto*, 2000; *Tréhu et al*., 2004; *Bahk et al*., 2013], so that this value likely will not underestimate potential CH_4 escape.

The amount and distribution of gas hydrate along the East Siberian slope is entirely conjectural, given the general lack of high-quality seismic lines and the absence of scientific boreholes. Following most literature, gas hydrate saturation is defined as being the volume fraction of gas hydrate within pore space. For the baseline Case A, we assume an initial gas hydrate saturation of 3% across the entire GHSZ below 6 mbsf. This gives an initial total mass of 29 Gt CH_4 (or 22 Gt of C) across the model domain. For comparison, *Biastoch et al*. [2011] assumed gas hydrate saturations of 2.4% (for Arctic slope sediments between 60°N and 70°N latitude) and 6.1% for such sediments north of 70°N.

Relatively few gas hydrate systems have been drilled to date [*Beaudoin et al*., 2014]. From such efforts, an average gas hydrate saturation of 3% is not unreasonable; for example, direct and indirect measurements indicate about this amount across the GHSZ on outer Blake Ridge, Hydrate Ridge, and the Ulleung Basin [*Paull and Matsumoto*, 2000; *Tréhu et al*., 2004; *Bahk et al*., 2013]. However, an estimate of 3% may be too high. We therefore offer three additional cases as potential starting distributions for gas hydrate. In Case B, we consider implications of glacial-interglacial variations in sea level, where during the last glacial maximum (LGM), the shallowest hydrate deposits could not have existed because of reduced pressure. A sensitivity test is also performed with an initial hydrate saturation of 5% and 1% (Cases C1 and C2). A complete list of model simulations is presented in Table 2, including sensitivity tests on sediment physical properties and geothermal heat flow (see supporting information). We note that drilling demonstrates that gas hydrate beneath the seafloor is often highly heterogeneous [e.g., *Paull and Matsumoto*, 2000; *Tréhu et al*., 2004; *Bahk et al*., 2013]. We have not incorporated this complexity into our modeling.

2.3. Model Spin-Up

Each model column was initialized without gas hydrate in the pore space until a steady state heat flow and hydrostatic pressure were attained. At this point, the subsurface temperature profile ($T(z)$) corresponds to a prescribed conductivity profile ($\lambda(z)$) and heat flow (q) according to:

$$q = \lambda(z)\frac{dT(z)}{dz},$$

where z is the depth below seafloor. Subsequently, for each sediment column, a preliminary depth for the base of the GHSZ (BGHSZ) was calculated, and a vertical distribution of gas hydrates was introduced within the stability zone. Because the thermal conductivity of gas hydrates is slightly higher than that of seawater [*Waite et al*., 2007; *Warzinski et al*., 2008; *Cortes et al*., 2009], the bulk thermal conductivity of sediment changes when gas hydrates are introduced, and the BGHSZ deepens. The adjusted BGHSZ depends on the prescribed gas hydrate saturation. For each column model run, this adjustment was determined through an intermediate iterative spin-up scheme whereby the BGHSZ was updated until a steady state was found, one consistent with the boundary conditions and the adjusted bulk thermal conductivity profile (supporting information Figure S1).

Model simulations were then run for 1000 years with a linear seafloor temperature increase of 3°C over the first 100 years of the simulation. The time step is adjusted internally in the model and is typically around 3 months during the dissociation phase with an upper limit preset to 1 year.

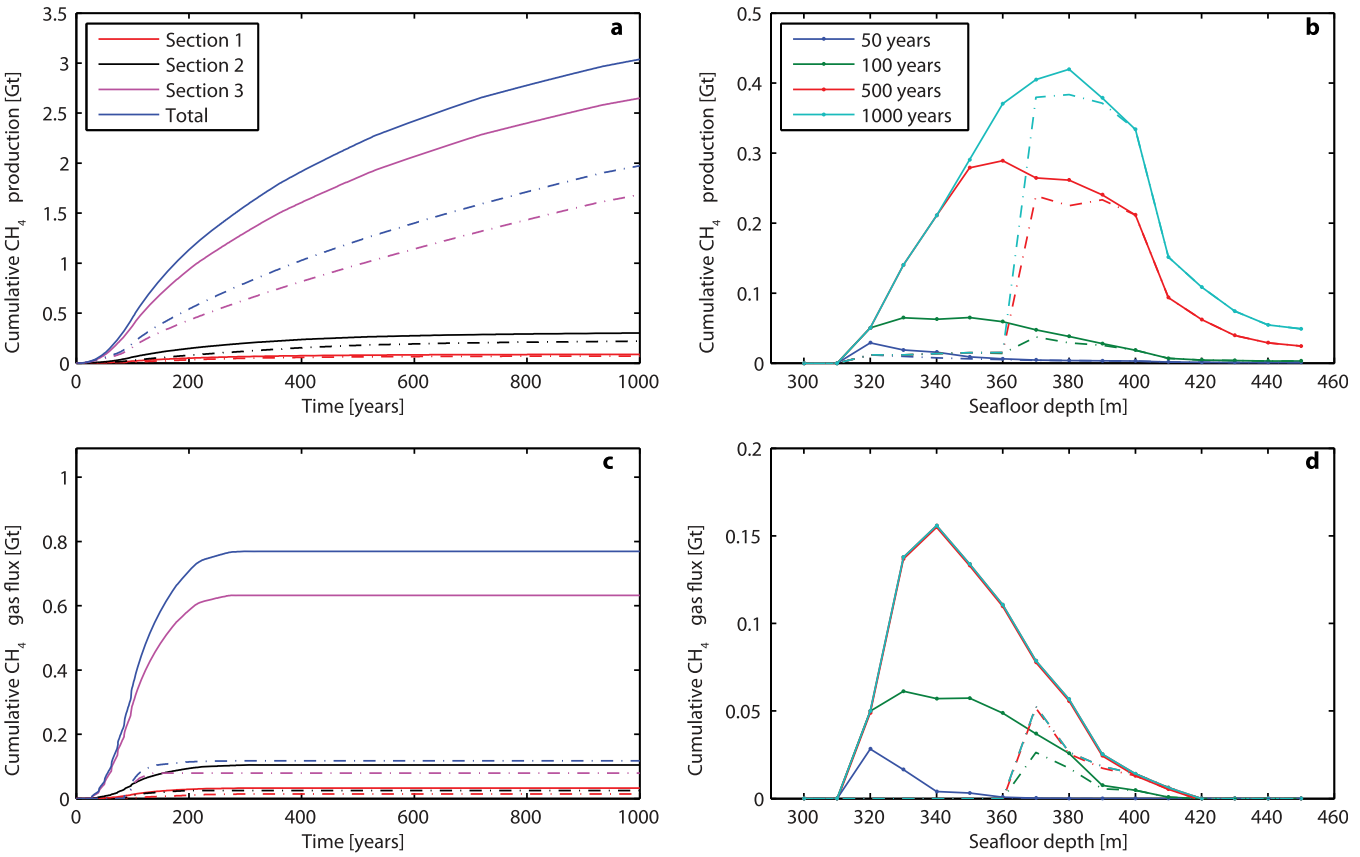

Figure 5. CH_4 production from hydrate dissociation and CH_4 fluxes. Case A solid curves and case B dashed curves showing (a) area integrated cumulative production for each section, (b) cumulative production within each depth interval (over all three sections) at different simulation times, (c) area integrated cumulative CH_4 gas release from the seafloor through fractures, and (d) cumulative CH_4 gas release through fractures within each depth interval (over all three sections) at different simulation times. Important to note that, since the low permeability restricts the migration of gas, no gas escapes through the porous media.

2.4. Fracture Formation Criteria

Crucially, the dissociation of gas hydrates and the ensuing production of free gas within pore space lead to increasing pore pressure, which could impact gas mobility within the sediments. In particular, fractures should form within the sediment column at some pore pressure threshold [*Daigle and Dugan*, 2010]. To account for this mechanical response, we make an offline estimate (i.e., the calculations are done after the model simulation) to determine the onset of sediment fracturing and enhanced CH_4 flow. Following *Daigle and Dugan* [2010], the normalized overpressure ratio ($\lambda^*(z)$), defined as the ratio of excess pore pressure to vertical effective stress under hydrostatic conditions, is calculated as follows:

$$\lambda^*(z) = \frac{P_{p(z)} - \rho_w g(d_{sf}+z)}{\sigma_{v(z)} - \rho_w g(d_{sf}+z)},$$

where P_p is the pore fluid pressure, ρ_w is the density of the pore fluid, g is the gravitational acceleration, d_{sf} is the seafloor depth, and σ_v is the total vertical stress given by

$$\sigma_{v(z)} = g \int \rho_{bulk}(z)\ dz,$$

and ρ_{bulk} is the sediment bulk density.

We assume that fractures occur when $\lambda^* \geq 0.6$, which implies that the pore pressure equals or exceeds the horizontal confining pressure if the horizontal stress is 60% of the vertical stress [*Daigle and Dugan*, 2010]. In our modeling, gas escape to the ocean through fractures occurs under one of two conditions: either (i) when λ^* in the top grid cell exceeds 0.6, or (ii) when overpressure within a confined unit exceeds the vertical effective stress ($\lambda^* \geq 1.0$), in which case fractures presumably propagate to the seafloor. As soon as

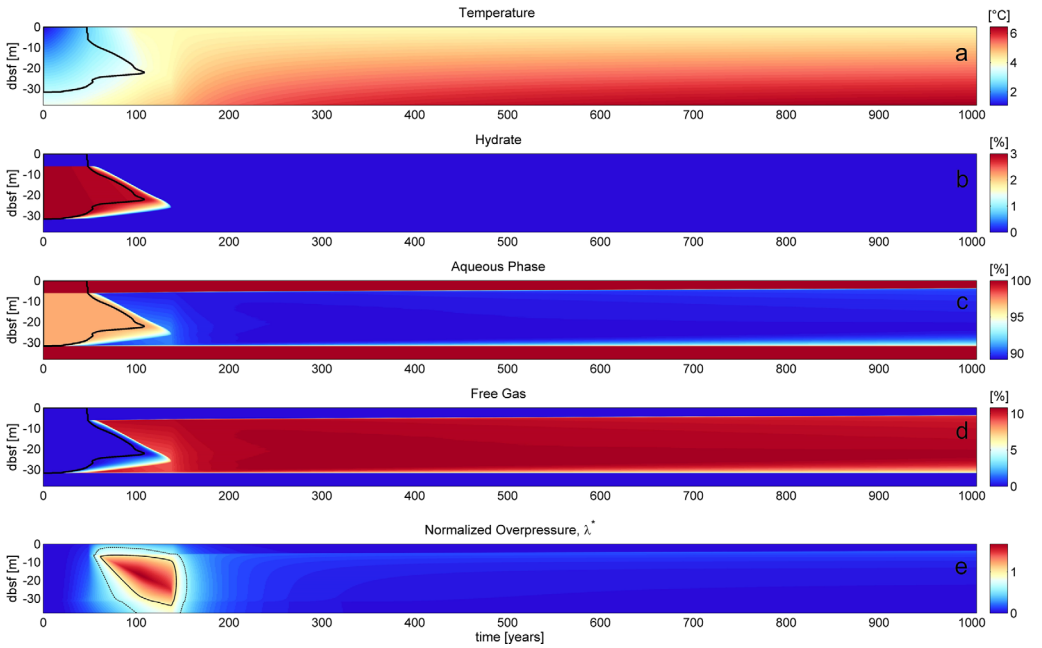

Figure 6. Example from Case A, section three at 360 mbsl. (a) The temperature and (b–d) the percentage of the pore space occupied by hydrates, aqueous phase, and gaseous phase respectively. (e) The normalized overpressure λ^*. Black solid lines in Figures 6a–6d indicate the GHSZ, and solid and dashed black lines in Figure 6e indicate the critical pressure criteria over which fractures form ($\lambda^* > 1.0$ and $\lambda^* > 0.6$, respectively). In this example, the hydrate deposit is completely dissociated at about 720 years into the simulation (Figure 6b) but the produced gas is not able to migrate to the seafloor through the porous media (Figure 6d). The gas production leads to a pore pressure exceeding the critical pressure in parts of the sediment column. Since λ^* exceeds 1.0 after about 70 years, fractures are assumed to connect instantly to the seafloor, and the gas down to ~10 mbsf is released directly into the ocean. The lower boundary of the assumed fractures is then propagating down through the sediment column with time continuously releasing any produced gas above, before eventually closing at about 175 years into the simulation. The $\lambda^* > 0.6$ isoline indicates that although fractures within the sediments stay open for a much longer period of time, these fractures do not reach the seafloor to enable gas release.

criterion (i) is met, all gas from the seafloor down to the grid cell where the criterion is no longer met escapes to the ocean. As soon as criterion (ii) is met, any gas above this point (the deepest grid cell meeting the criterion) escapes to the ocean. In either case, all gas within the fractured zone enters the ocean within one time step.

A consequence of this offline approach is that the pressure field does not dynamically react to gas escape through fractures (because the calculations are performed after the model simulation is finished). More likely, pressure relief would occur when gas starts to migrate. This should lead to higher gas hydrate dissociation rates due to lower-pressure conditions at a given temperature. Fractures might also close after pressure relief, allowing in situ pressure to rise and fractures to open and close over time [e.g., *Scandella et al.*, 2011].

Taken together, our modeled estimates for gas transport and CH_4 release to the seafloor through fractures should be viewed as an upper limit, both quantitatively and in terms of timing. Moreover, the amount of CH_4 that can escape must be lower than the total amount of gas produced from hydrate dissociation. Thus, we are placing a new constraint on gas escape that is lower than estimates based simply on the vertical displacement of the BGHSZ [e.g., *Biastoch et al.*, 2011].

3. Results and Discussion

3.1. Baseline Model Simulation (Case A)

During the first 100 years, gas hydrate dissociation produces ~0.5 Gt of CH_4 (Figure 5a), most of which occurs within section three due to the larger slope area (Figure 3). After 100 years, all gas hydrate in sediment above 320 mbsl dissociates. At deeper water depths, complete dissociation of gas hydrate takes longer; for example, this outcome requires at least 500 years when depths exceed 350 m (Figure 5b). This is because of the more stable pressure conditions, the deeper initial BGHSZ and the time to propagate heat

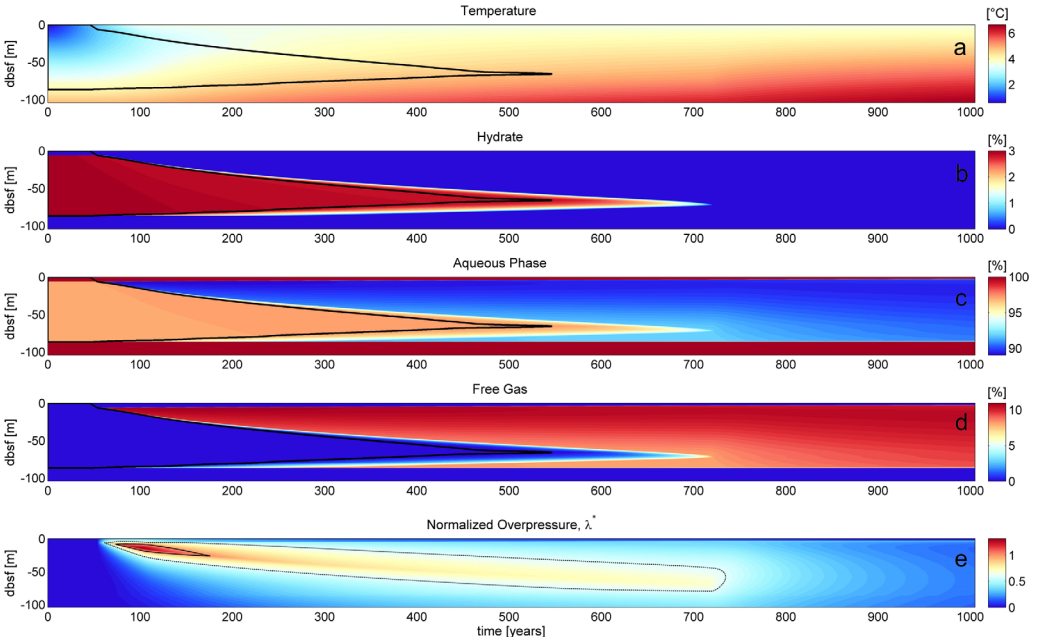

Figure 7. Example from Case A, section one at 380 mbsl. (a) The temperature and (b–d) the percentage of the pore space occupied by hydrates, aqueous phase, and gaseous phase, respectively. (e) The normalized overpressure λ^*. Black solid lines in Figures 7a–7d indicate the GHSZ, and solid and dashed black lines in Figure 7e indicates the critical pressure criteria over which fractures form ($\lambda^* > 1.0$ and $\lambda^* > 0.6$, respectively). In this example, the hydrate deposit is completely dissociated at about 140 years into the simulation (Figure 7b). The produced gas is not able to migrate to the seafloor through the porous media (Figure 7d). The gas production leads to a pore pressure exceeding the critical pressure in parts of the sediment column. Since λ^* exceeds 1.0 after about 60 years, fractures are assumed to connect instantly to the seafloor, and the gas down to ~7 mbsf is released directly into the ocean. The lower boundary of the assumed fractures is then propagating down through the sediment column with time continuously releasing any produced gas above, before eventually closing at about 140 years into the simulation. Note that the hydrate deposit in this example is shallower and less stable than the example in Figure 4 even though the seafloor depth is larger, a consequence of the higher seafloor temperature in this section (supporting information Table S1).

downward from the seafloor. At 450 mbsl, the BGHSZ does not rise to the topmost occurrence of gas hydrate in any of the three sections, even after 1000 years.

Importantly, the low permeability of the sediments (ranging from about 10^{-17} m^2 at 100 mbsf to about $3 \cdot \times 10^{-16}$ m^2 at the seafloor, Figure 4) impedes the mobility of the produced gas. In Case A, no CH_4 escapes the seafloor through porous media (Figures 6d and 7d). However, gas production in the sediment increases the pore pressure around gas hydrate dissociation fronts, such that criteria for developing sediment fractures are exceeded. Fractures then connect to the seafloor and release CH_4 gas after 25 years (Figures 5c and 5d). The cumulative CH_4 release after 100 years is 0.35 Gt (Figure 5c), which corresponds to an annual release of 0.6% of the present-day global atmospheric CH_4 budget of ~0.6 Gt CH_4 yr^{-1} [*Solomon*, 2007].

These basic results change slightly with modifications to the initial gas hydrate saturation or the physical and geothermal properties of the sediments (see supporting information). For example, in Case C1 (5% hydrate saturation), the cumulative CH_4 gas flux to the seafloor increases to 0.46 Gt after 100 years (Figure 8).

3.1.1. Implications of Glacial-Interglacial Variations in Sea Level (Case B)

The shallowest water depths where gas hydrates can occur within modeled slope sections one, two, and three are 350, 340, and 320 m, respectively. These differences arise from regional variations in seafloor temperature. However, the mean relative sea level during the LGM (defined here as 20,000 years before present) was significantly lower. Through nearest neighbor interpolations of the ICE6G data set [*Peltier et al.*, 2015], the local relative sea level was found to be about 110 m lower than present in all three sections. Assuming similar seafloor temperatures during the LGM, the reduction in sea level-induced pressure would mean that gas hydrate could not exist in sediment within the three slope sections 20,000 years ago at seafloor depths shallower than 460, 450, and 430 mbsl at present day (Figure 9).

A deepening of the warm Atlantic layer may have decreased bottom water temperatures along the upper slope of the Arctic during the last glacial cycle [*Cronin et al.*, 2012]. Using the T+H model, we find that a 2°C

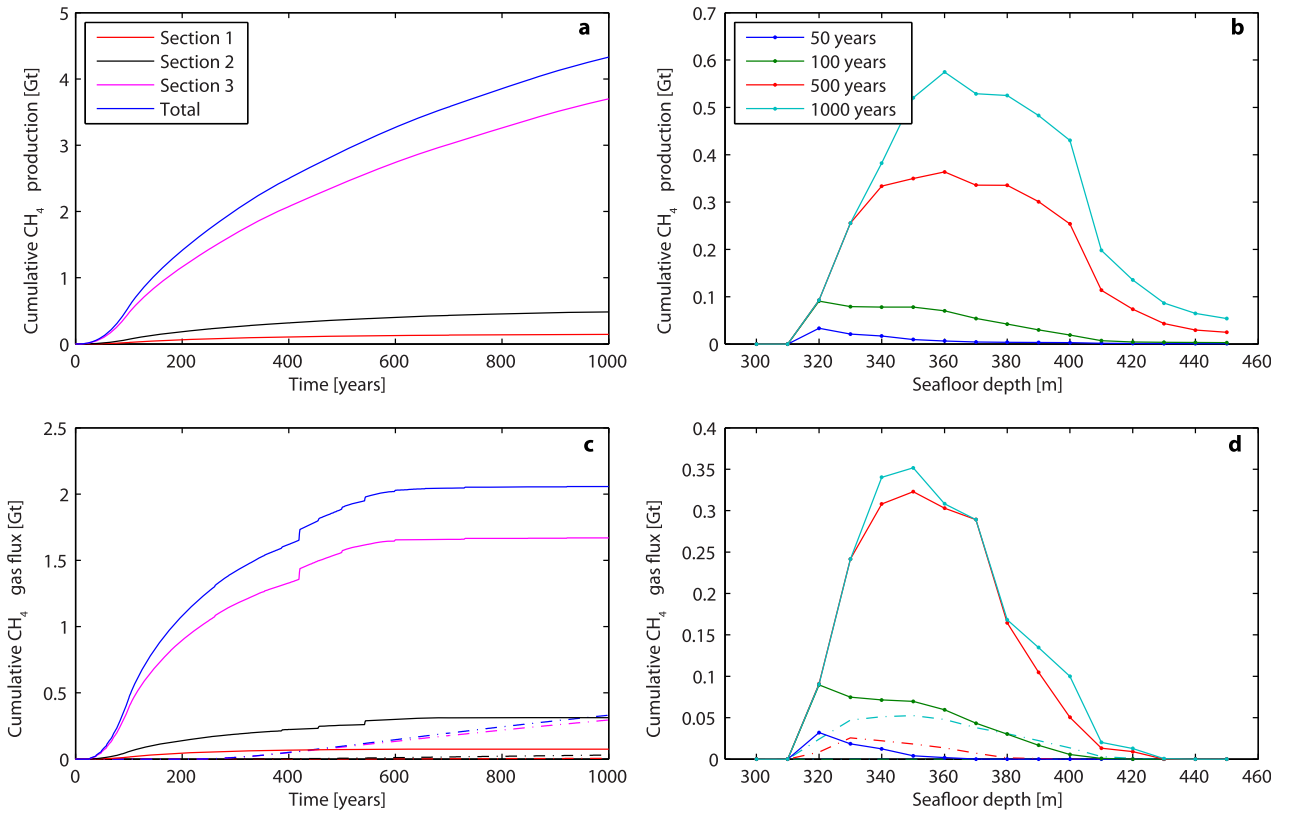

Figure 8. CH_4 production from hydrate dissociation and CH_4 fluxes from Case C1, showing (a) area integrated cumulative production for each section, (b) cumulative production within each depth interval (over all three sections) at different simulation times, (c) area integrated cumulative CH_4 gas release from the seafloor, and (d) cumulative CH_4 gas release within each depth interval (over all three sections) at different simulation times. Solid/dashed curves in Figures 8c and 8d are gas flux through fractures/porous media. Note that the gas release through fractures (which is calculated offline after the simulation) and through porous media cannot be added to get a total flux since much of the porous media flux would have already been lost through the fractures. The modeled flux is dominated by fracture flow however.

cooling of bottom waters would partly compensate for lowered sea level (about 70 m). The minimum seafloor depths for gas hydrate occurrence noted above therefore may have been around 390, 380, and 360 mbsl for the three sections.

Assuming twice the gas hydrate formation rate of 7.7 mmol CH_4 m^{-2} yr^{-1} presented by *Wallmann et al.* [2012], about 5.2 kg/m^2 CH_4 would have formed over the last 20,000 years. The reason for doubling the formation rate is to compensate for possibly higher input of organic matter to the sediments and possible thermogenic CH_4 sources in the region. Initializing the simulation with a total hydrate accumulation of 5.2 kg/m^2 CH_4 in the depleted depth ranges (corresponding to hydrate saturations between 0.1 and 2.7% depending on the position of the BGHSZ) and a hydrate saturation of 3% within the GHSZ for the remaining shelf slope down to 450 mbsl (Case B) the initial hydrate reservoir mass is reduced from 29 Gt (Case A) to 21 Gt CH_4. In Case B, the total CH_4 produced through gas hydrate dissociation is 0.2 Gt after 100 years. The difference from Case A (0.5 Gt) occurs because the gas hydrate most susceptible to bottom water warming exists at shallow water depths, but these areas are already partly depleted in gas hydrate from previous LGM conditions. Even after 1000 years, the amount of CH_4 produced through dissociation is significantly smaller; 2.0 Gt compared to 3.0 (about 30%) (Figures 5a and 5b). The estimates for CH_4 release to the seafloor also are reduced drastically, from 0.35–0.8 Gt CH_4 (Case A) to 0.05–0.1 Gt (Case B) after 100–1000 years (Figures 5c and 5d). We note that this simulation does not consider more recent warming episodes in the Arctic, such as during the early Holocene insolation maximum [*Stranne et al.*, 2014]. Such intervals may have depleted the "feather edge" of the modern GHSZ further, somewhat analogous to the effect of the lower sea levels during LGM.

3.2. Comparison With Other Results

A series of papers have considered the response of marine gas hydrate systems to an increase in bottom water temperature, both for marine sediment in general and for the Arctic in particular. *Xu et al.* [2001]

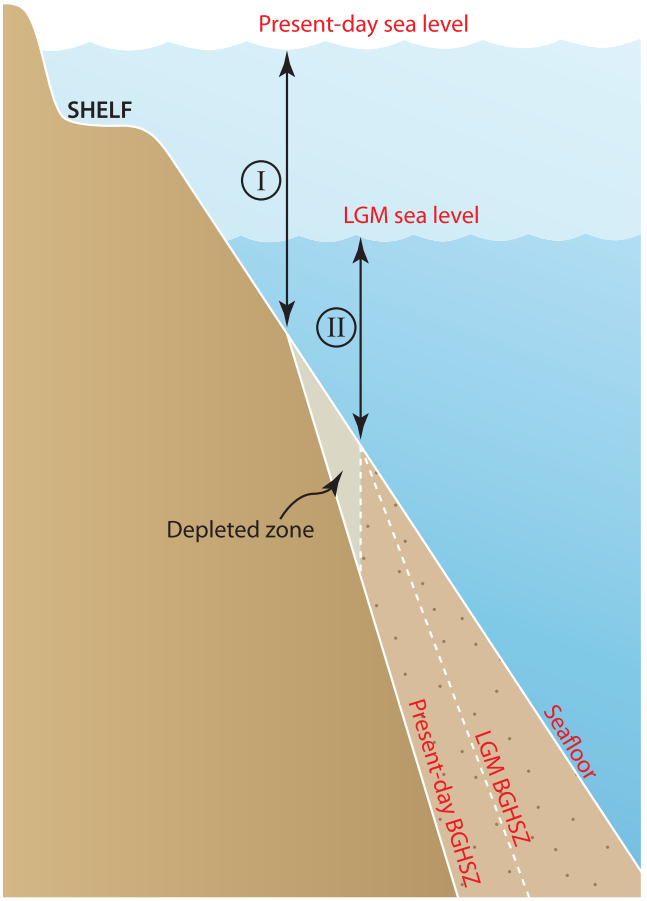

Figure 9. Schematic sketch showing the effect of lower sea levels during LGM on Arctic hydrate deposits. The gray triangle indicates a zone which is assumed to have been depleted during LGM. In the depleted zone, hydrates are assumed to have accumulated over 20,000 years with twice the formation rate presented by *Wallmann et al.* [2012]. Note that we also assume that, although hydrate deposits situated at depths greater than the LGM minimum seafloor depth (II) would be partly dissociated, the remaining hydrates would act as a lid to obstruct CH_4 gas from migrating to the seafloor. Note also that the LGM minimum seafloor depth (II) is smaller than the present-day minimum seafloor depth (I) due to assumed colder seafloor temperatures during LGM.

presented a 1-D modeling perspective for the overall process. Even though our modeling incorporates numerous additional factors, the results are consistent with their two main conclusions. The BGHSZ shoals and gas hydrate within sediment dissociates, but only after a significant time lag, because of relatively slow heat propagation.

Biastoch et al. [2011] presented estimates for CH_4 escape from Arctic margins above 60°N. The estimates were based on a GHSZ with initial gas hydrate saturations of between 2.4% and 6.1%, a seafloor temperature increase of 1–2°C over 100 years, and fully equilibrated changes in the thickness of the GHSZ. The starting mass of CH_4 within gas hydrate north of 60°N was 1200 Gt CH_4, and they concluded that 16 Gt CH_4 might escape the seafloor over 100 years, and 130 Gt CH_4 might escape once new steady state conditions were reached.

Kretschmer et al. [2015] used a similar approach to estimate CH_4 escape from the global hydrate inventory due to ocean warming over the next 100 years. However, starting gas hydrate saturations were much less than in the study by *Biastoch et al.* [2011]; indeed, they were about 2 orders of magnitude lower for the Arctic region. For our study area, *Kretschmer et al.* [2015] indicate very low fluxes of CH_4 to the ocean. While consistent with our results, the similarity seems to reflect mostly less ocean warming (<1°C) and much lower gas hydrate abundance.

Although gas hydrate dissociation can be modeled by calculating the shift in the BGHSZ over time, assuming a conductive heat flow and that the hydrate deposit is in constant equilibrium [e.g., *Biastoch et al.*, 2011; *Kretschmer et al.*, 2015], such approach should overestimate gas hydrate dissociation rates. Gas hydrate dissociation is an endothermic reaction, which consumes heat, and thus decreases the rate of dissociation for a given warming of the seafloor. Gas hydrate dissociation also releases fresh water, which decreases the salinity, and free gas, which increases the pressure around dissociation fronts. Both processes act to stabilize gas hydrates on at least modest time scales. More crucially, simple approaches do not consider free gas mobility within fine-grained sediments of low permeability. These processes are incorporated into the T+H model, and they have a substantial impact on the amount of CH_4 that can escape from the seafloor over centennial time scales.

Phrampus et al. [2014] used a conductive heat flow model to simulate the steady state base of the GHSZ on the upper slope of the Alaskan Beaufort margin, principally to understand a discrepancy between predicted depths and observed depths for bottom simulating reflectors that mark the BGHSZ in this area. They mostly attribute the discrepancy to recent warming of bottom water temperatures (~0.5°C) and dissociation of gas

hydrate in underlying sediment. Based on this finding, they conclude that significant amounts of CH_4 might escape the seafloor in the coming century, but with several key assumptions, one being that sediments only retain 10% of the gas produced during gas hydrate dissociation.

The T+H model includes multiphase flow dynamics that influence gas mobility. One can then define sediment gas retention (SGR) as:

$$\mathrm{SGR}=1-\frac{cumulative\ \ gas\ \ flux}{cumulative\ \ gas\ \ production},$$

where SGR can be calculated for the sediment column at any given time. Without considering sediment fractures, the SGR is 100% in Cases A and B, and close to 100% in Case C. Even when CH_4 escape happens through sediment fractures, such as in Case B, the SGR is around 70% after 100 years, and approaches 95% over the remaining part of the simulation. The increase in SGR occurs because while CH_4 dissociation takes place (although at diminishing rates) throughout the simulation (Figure 5a), in situ pressure is not high enough to allow for gas transport through fractures after ~200 years and forward (Figure 5c). While the uncertainties are large due to the crude representation of sediment fracturing, such values emphasize that gas retention within sediments is of comparable importance to constraining seafloor CH_4 release as the total amount of CH_4 produced from gas hydrate dissociation.

The T+H model has been used previously to investigate thermal dissociation of gas hydrate and seafloor CH_4 release from other margins of the Arctic [*Reagan and Moridis*, 2009; *Marín-Moreno et al*., 2013; *Thatcher et al*., 2013]. The latter two studies investigated whether observed bubble plumes on the upper slope west of Svalbard [*Westbrook et al*., 2009] might be associated with an overall 30 year increase in local seafloor temperature and gas hydrate dissociation. Even though this idea has been challenged by *Berndt et al*. [2014], who suggest that active CH_4 seepage in this area has occurred for at least 1000 years, the modeling results are intriguing. To have bottom water warming drive CH_4 escape within 30 years, *Thatcher et al*. [2013] suggested that a combination of very high sediment permeability ($>10^{-13}$ m^2), a thin shallow zone without gas hydrate (<5 m), and a high gas hydrate saturation (>5%) was needed. Our model results augment this finding. For example, in our baseline Case A, a relatively short 30 year time lag between the onset of seafloor warming and CH_4 escape can occur with lower gas hydrate saturation (3%) and much lower permeability ($<10^{-16}$ m^2). However, this is only when sediment fractures are considered. That is, there is no need to arbitrarily raise the permeability of the sediments.

Archer [2015] recently presented model results for CH_4 cycling on the Siberian continental margin over long time scales. One conclusion is that the abundance of gas hydrate today depends on the evolution of the GHSZ (because of changes in sea-level and temperature) as well as CH_4 inputs and outputs over time. A second conclusion is that while the model results are sensitive to the assumed CH_4 production rates, these are poorly constrained. This conclusion seem valid on longer time scales but our results show that on decadal to centennial time scales the present-day hydrate distribution (which is a strong function of long-term CH_4 production rates) is of less importance in terms of CH_4 production from anthropogenic warming-induced gas hydrate dissociation. This is related to the fact that the dissociation process is endothermic. During the first part of our simulations, the dissociation rate probably approaches the upper limit, as imposed by the rate of warming (3°C over 100 years), and is therefore less sensitive to sediment hydrate saturation (supporting information Figure S3).

Perhaps the most interesting result from our study is the importance of sediment fractures. Effectively, very little CH_4 can escape the seafloor without the formation of conduits with high permeability. This finding is irrespective of the gas hydrate content.

3.3. Model Uncertainties

As should be clear, there are several uncertainties in our modeling. The basic ones include boundary conditions (e.g., spatial variability of hydrate distribution, saturation states, and variations in sediment physical properties) and processes missing in the modeling (e.g., oxidation of CH_4 at the base of the SRZ). The more fundamental issue is how to properly model the formation of sediment fractures and the transport of CH_4 through such fractures.

The modeling does not account for free gas that may currently be trapped beneath the GHSZ, or actively migrating into it from deeper levels. In a study at Vestnesa Ridge north-west of Svalbard, it is suggested

that chimneys fed by critically pressured gas beneath can facilitate free gas migration through the GHSZ [*Smith et al*., 2014]. It is important to note, however, that up to 90% or more of the CH_4 that reaches the SRZ may be consumed by anaerobic CH_4 oxidation [e.g., *Hinrichs and Boetius*, 2002; *Knittel and Boetius*, 2009]. Also, at water depths greater than 100 m, considerable quantities of CH_4 can either be dissolved in water [*McGinnis et al*., 2006] or consumed by microbes [*Dickens*, 2001a]. Because the shallowest seafloor depths where stable hydrates can exist in the present study area is 320 mbsl, it is likely that much of the CH_4 gas that could escape sediments and the SRZ would not reach the atmosphere.

4. Conclusions

Our dynamic modeling suggests an important inertia of gas hydrate systems to seafloor warming, whether gas hydrates occur along the East Siberian continental slope or elsewhere. Gas hydrate dissociation occurs relatively slowly, because the reaction is endothermic, it decreases pore water salinity, and it increases local pore pressure. Gas hydrate is also likely depleted from sediment on the upper slope of many modern continental margins (the most susceptible region), a legacy of sea level changes during the Pleistocene. More crucially, permeable pathways need to form in order for free CH_4 gas to escape the seafloor. Previous estimates for CH_4 fluxes from anthropogenic warming-induced gas hydrate dissociation along Arctic margins based solely on changes in the thickness of the GHSZ probably overestimate these fluxes considerably. This is because CH_4 production from gas hydrate dissociation is reduced over the short term (100 years) when taking into account "retarding effects" and an already partly depleted gas hydrate reservoir. Our results show that gas production from hydrate dissociation is reduced by 60% (to 0.2 Gt) and the gas flux is reduced by over 80% (to 0.05 Gt) over the first 100 years when taking into account a partly depleted hydrate reservoir from lower sea levels during LGM. Moreover, after 100 years, $>$70% of the produced gas from hydrate dissociation still resides within the sediments. Given that seafloor CH_4 release has been widely invoked to explain negative carbon isotope excursions in the geological record [e.g., *Dickens*, 2003], it may be fruitful to conduct such modeling over longer time scales to see whether these scenarios are realistic.

Acknowledgments
Research grants to individual scientist were provided by the Swedish Research Council (VR) and Knut and Alice Wallenberg Foundation. We thank C. Pearce and M. Reagan for valuable input. All data supporting the figures and text of this manuscript are available upon request from the corresponding author.

References

Archer, D. (2007), Methane hydrate stability and anthropogenic climate change, *Biogeosciences*, *4*(4), 521–544, doi:10.5194/bg-4-521-2007.

Archer, D. (2015), A model of the methane cycle, permafrost, and hydrology of the Siberian continental margin, *Biogeosciences*, *12*(10), 2953–2974, doi:10.5194/bg-12-2953-2015.

Bahk, J.-J., G.-Y. Kim, J.-H. Chun, J.-H. Kim, J. Y. Lee, B.-J. Ryu, J.-H. Lee, B.-K. Son, and T. S. Collett (2013), Characterization of gas hydrate reservoirs by integration of core and log data in the Ulleung Basin, East Sea, *Mar. Pet. Geol.*, *47*, 30–42, doi:10.1016/j.marpetgeo.2013.05.007.

Beaudoin, Y. C., W. Waite, R. Boswell, and S. R. Dallimore (Eds.) (2014), *Frozen Heat: A UNEP Global Outlook on Methane Gas Hydrates*, vol. 1, 77 pp., U. N. Environ. Programme, GRID-Arendal, Norway.

Berndt, C. et al. (2014), Temporal constraints on hydrate-controlled methane seepage off Svalbard, *Science*, *343*(6168), 284–287, doi:10.1126/science.1246298.

Bhatnagar, G., S. Chatterjee, W. G. Chapman, B. Dugan, G. R. Dickens, and G. J. Hirasaki (2011), Analytical theory relating the depth of the sulfate-methane transition to gas hydrate distribution and saturation, *Geochem. Geophys. Geosyst.*, *12*, Q03003, doi:10.1029/2010GC003397.

Biastoch, A., et al. (2011), Rising Arctic Ocean temperatures cause gas hydrate destabilization and ocean acidification, *Geophys. Res. Lett.*, *38*, L08602, doi:10.1029/2011GL047222.

Collett, T. S., K. J. Bird, K. A. Kvenvolden, and L. B. Magoon (1988), Geologic interrelations relative to gas hydrates within the North Slope of Alaska, *U.S. Geol. Surv. Open File Rep.*, *88-389*, 150 pp.

Cortes, D. D., A. I. Martin, T. S. Yun, F. M. Francisca, J. C. Santamarina, and C. Ruppel (2009), Thermal conductivity of hydrate-bearing sediments, *J. Geophys. Res.*, *114*, B11103, doi:10.1029/2008JB006235.

Cronin, T. M., G. S. Dwyer, J. Farmer, H. A. Bauch, R. F. Spielhagen, M. Jakobsson, J. Nilsson, W. M. Briggs Jr., and A. Stepanova (2012), Deep Arctic Ocean warming during the last glacial cycle, *Nat. Geosci.*, *5*(9), 631–634, doi:10.1038/ngeo1557.

Daigle, H., and B. Dugan (2010), Origin and evolution of fracture-hosted methane hydrate deposits, *J. Geophys. Res.*, *115*, B11103, doi:10.1029/2010JB007492.

Dickens, G. (2001), On the fate of past gas: What happens to methane released from a bacterially mediated gas hydrate capacitor?, *Geochem. Geophys. Geosyst.*, *2*(1), 1037, doi:10.1029/2000GC000131.

Dickens, G. R. (2001), The potential volume of oceanic methane hydrates with variable external conditions, *Org. Geochem.*, *32*(10), 1179–1193, doi:10.1016/S0146-6380(01)00086-9.

Dickens, G. R. (2003), Rethinking the global carbon cycle with a large, dynamic and microbially mediated gas hydrate capacitor, *Earth Planet. Sci. Lett.*, *213*(3–4), 169–183, doi:10.1016/S0012-821X(03)00325-X.

Dickens, G. R., and M. S. Quinby-Hunt (1997), Methane hydrate stability in pore water: A simple theoretical approach for geophysical applications, *J. Geophys. Res.*, *102*(B1), 773–783, doi:10.1029/96JB02941.

Drachev, S. S. (2011), Chapter 25 Tectonic setting, structure and petroleum geology of the Siberian Arctic offshore sedimentary basins, *Geol. Soc. London Mem.*, *35*(1), 369–394, doi:10.1144/M35.25.

Elliott, S., M. Reagan, G. Moridis, and P. C. Smith (2010), Geochemistry of clathrate-derived methane in Arctic Ocean waters, *Geophys. Res. Lett.*, *37*, L12607, doi:10.1029/2010GL043369.
Elliott, S., M. Maltrud, M. Reagan, G. Moridis, and P. Cameron-Smith (2011), Marine methane cycle simulations for the period of early global warming, *J. Geophys. Res.*, *116*, G01010, doi:10.1029/2010JG001300.
Ferré, B., J. Mienert, and T. Feseker (2012), Ocean temperature variability for the past 60 years on the Norwegian-Svalbard margin influences gas hydrate stability on human time scales, *J. Geophys. Res.*, *117*, C10017, doi:10.1029/2012JC008300.
Giustiniani, M., U. Tinivella, M. Jakobsson, M. Rebesco, M. Giustiniani, U. Tinivella, M. Jakobsson, and M. Rebesco (2013), Arctic Ocean gas hydrate stability in a changing climate, *J. Geol. Res.*, *2013*, e783969, doi:10.1155/2013/783969.
Gosnold, W. D., and B. Panda (2002), *The Global Heat Flow Database of the International Heat Flow Commission*. [Available at http://www.und.edu/org/ihfc/index2.html.]
Grantz, A., and D. A. Dinter (1980), Constraints of geologic processes on western Beaufort Sea oil developments, *Oil Gas J.*, *78*(18), 304–319.
Handa, Y. P. (1990), Effect of hydrostatic pressure and salinity on the stability of gas hydrates, *J. Phys. Chem.*, *94*(6), 2652–2657, doi:10.1021/j100369a077.
Hester, K. C., and P. G. Brewer (2009), Clathrate hydrates in nature, *Annu. Rev. Mar. Sci.*, *1*(1), 303–327, doi:10.1146/annurev.marine.010908.163824.
Hinrichs, K.-U., and A. Boetius (2002), The anaerobic oxidation of methane: New insights in microbial ecology and biogeochemistry, in *Ocean Margin Systems*, edited by P. D. G. Wefer et al., pp. 457–477, Springer, Berlin.
Isaksen, I. S. A., M. Gauss, G. Myhre, K. M. Walter Anthony, and C. Ruppel (2011), Strong atmospheric chemistry feedback to climate warming from Arctic methane emissions, *Global Biogeochem. Cycles*, *25*, GB2002, doi:10.1029/2010GB003845.
Jakobsson, M., et al. (2012), The international bathymetric chart of the Arctic Ocean (IBCAO) version 3.0, *Geophys. Res. Lett.*, *39*, L12609, doi:10.1029/2012GL052219.
Khain, V. E., I. D. Polyakova, and N. I. Filatova (2009), Tectonics and petroleum potential of the East Arctic province, *Russ. Geol. Geophys.*, *50*(4), 334–345, doi:10.1016/j.rgg.2009.03.006.
Knittel, K., and A. Boetius (2009), Anaerobic oxidation of methane: Progress with an unknown process, *Annu. Rev. Microbiol.*, *63*(1), 311–334, doi:10.1146/annurev.micro.61.080706.093130.
Kretschmer, K., A. Biastoch, L. Rüpke, and E. Burwicz (2015), Modeling the fate of methane hydrates under global warming, *Global Biogeochem. Cycles*, *29*, 610–625, doi:10.1002/2014GB005011.
Kvenvolden, K. A. (1989), Methane hydrates and global climate, *Global Biogeochem. Cycles, 2(3), 221-229.*
Kvenvolden, K. A., and A. Grantz (1990), Gas hydrates of the Arctic Ocean region, in edited by A. Grantz, L. Johnson, and J. F. Sweeney, *Arctic Ocean Region, Geol. Soc. Am.*, Boulder, Colo., 539–549.
Liang-Guang Tang, X.-S. L. (2006), Control mechanisms for gas hydrate production by depressurization in different scale hydrate reservoirs, *Energy Fuels*, *21*(1), 227–233, doi:10.1021/ef0601869.
Locarnini, R. A., et al. (2013), *World Ocean Atlas 2013*, vol. 1, *Temperature*, edited by S. Levitus, NOAA Atlas NESDIS, vol. 73, 40 pp., U.S. Govern. Print. Off., Washington, D. C.
Lunt, D. J., A. Ridgwell, A. Sluijs, J. Zachos, S. Hunter, and A. Haywood (2011), A model for orbital pacing of methane hydrate destabilization during the Palaeogene, *Nat. Geosci.*, *4*(11), 775–778, doi:10.1038/ngeo1266.
Marín-Moreno, H., T. A. Minshull, G. K. Westbrook, B. Sinha, and S. Sarkar (2013), The response of methane hydrate beneath the seabed offshore Svalbard to ocean warming during the next three centuries, *Geophys. Res. Lett.*, *40*, 5159–5163, doi:10.1002/grl.50985.
Max, M. D., and A. Lowrie (1993), Natural gas hydrates: Arctic and Nordic Sea potential, in edited by T. O. Vorren, et al., Arctic Geology and Petroleum Potential, NPF Special Publication 2, pp. 27–53, Elsevier, Amsterdam.
McGinnis, D. F., J. Greinert, Y. Artemov, S. E. Beaubien, and A. Wüest (2006), Fate of rising methane bubbles in stratified waters: How much methane reaches the atmosphere?, *J. Geophys. Res.*, *111*, C09007, doi:10.1029/2005JC003183.
Milkov, A. V. (2004), Global estimates of hydrate-bound gas in marine sediments: How much is really out there?, *Earth Sci. Rev.*, *66*(3–4), 183–197, doi:10.1016/j.earscirev.2003.11.002.
Moridis, G. J., M. B. Kowalsky, and K. Pruess (2014), *TOUGH+HYDRATE v1.0 User's Manual: a code for the simulation of System behavior in hydrate-bearing geologic media*, Report LBNL-0149E, Lawrence Berkeley National Laboratory, Berkeley, Calif.
Moridis, G. J., T. S. Collett, S. R. Dallimore, T. Inoue, and T. Mroz (2005), Analysis and interpretation of the thermal test of gas hydrate dissociation in the JAPEX/JNOC/GSC et al. Mallik 5L-38 gas hydrate production research well, *Bull. Geol. Surv. Can.*, *585*, 140.
Paull, C. K., and R. Matsumoto (2000), 1. Leg 164 overview, in *Proceedings of the Ocean Drilling Program. Scientific Results*, vol. 164, pp. 3–10, Ocean Drill. Program, College Station, Tex.
Paull, C. K., W. Ussler, and W. P. Dillon (1991), Is the extent of glaciation limited by marine gas-hydrates?, *Geophys. Res. Lett.*, *18*(3), 432–434, doi:10.1029/91GL00351.
Peltier, W. R., D. F. Argus, and R. Drummond (2015), Space geodesy constrains ice age terminal deglaciation: The global ICE-6G_C (VM5a) model, *J. Geophys. Res. Solid Earth*, *120*, 450–487, doi:10.1002/2014JB011176.
Phrampus, B. J., M. J. Hornbach, C. D. Ruppel, and P. E. Hart (2014), Widespread gas hydrate instability on the upper U.S. Beaufort margin, *J. Geophys. Res. Solid Earth*, *119*, 8594–8609, doi:10.1002/2014JB011290.
Pollack, H. N., S. J. Hurter, and J. R. Johnson (1993), Heat flow from the Earth's interior: Analysis of the global data set, *Rev. Geophys.*, *31*(3), 267–280, doi:10.1029/93RG01249.
Polyakov, I., et al. (2007), Observational program tracks Arctic Ocean transition to a warmer state, *Eos Trans. AGU*, *88*(40), 398–399, doi:10.1029/2007EO400002.
Posewang, J., and J. Mienert (1999), High-resolution seismic studies of gas hydrates west of Svalbard, *Geo Mar. Lett.*, *19*(1-2), 150–156, doi:10.1007/s003670050102.
Reagan, M. T., and G. J. Moridis (2008), Dynamic response of oceanic hydrate deposits to ocean temperature change, *J. Geophys. Res.*, *113*, C12023, doi:10.1029/2008JC004938.
Reagan, M. T., and G. J. Moridis (2009), Large-scale simulation of methane hydrate dissociation along the West Spitsbergen Margin, *Geophys. Res. Lett.*, *36*, L23612, doi:10.1029/2009GL041332.
Reagan, M. T., G. J. Moridis, S. M. Elliott, and M. Maltrud (2011), Contribution of oceanic gas hydrate dissociation to the formation of Arctic Ocean methane plumes, *J. Geophys. Res.*, *116*, C09014, doi:10.1029/2011JC007189.
Ruppel, C., G. R. Dickens, D. G. Castellini, W. Gilhooly, and D. Lizarralde (2005), Heat and salt inhibition of gas hydrate formation in the northern Gulf of Mexico, *Geophys. Res. Lett.*, *32*, L04605, doi:10.1029/2004GL021909.
Ruppel, C. D. (2011), Methane hydrates and contemporary climate change, *Nat. Educ. Knowledge*, *3*(10), *29*.
Sassen, R., S. T. Sweet, A. V. Milkov, D. A. DeFreitas, and M. C. Kennicutt (2001), Thermogenic vent gas and gas hydrate in the Gulf of Mexico slope: Is gas hydrate decomposition significant?, *Geology*, *29*(2), 107–110, doi: 10.1130/0091-7613(2001)029<0107:TVGAGH>2.0.CO;2.

Scandella, B. P., C. Varadharajan, H. F. Hemond, C. Ruppel, and R. Juanes (2011), A conduit dilation model of methane venting from lake sediments, *Geophys. Res. Lett.*, *38*, L06408, doi:10.1029/2011GL046768.

Serreze, M. C., and R. G. Barry (2011), Processes and impacts of Arctic amplification: A research synthesis, *Global Planet. Change*, *77*(1–2), 85–96, doi:10.1016/j.gloplacha.2011.03.004.

Shakhova, N., et al. (2015), The East Siberian Arctic Shelf: Towards further assessment of permafrost-related methane fluxes and role of sea ice, *Philos. Trans. R. Soc. A*, *373*(2052), 20140451, doi:10.1098/rsta.2014.0451.

Smith, A. J., J. Mienert, S. Bünz, and J. Greinert (2014), Thermogenic methane injection via bubble transport into the upper Arctic Ocean from the hydrate-charged Vestnesa Ridge, Svalbard, *Geochem. Geophys. Geosyst.*, *15*(5), 1945–1959, doi:10.1002/2013GC005179.

Solomon, S. (2007), Climate change 2007-the physical science basis: Working group I contribution to the fourth assessment report of the IPCC, Cambridge University Press.

Stranne, C., M. Jakobsson, and G. Björk (2014), Arctic Ocean perennial sea ice breakdown during the Early Holocene Insolation Maximum, *Quat. Sci. Rev.*, *92*, 123–132, doi:10.1016/j.quascirev.2013.10.022.

Stranne, C., and M. O'Regan (2015), Conductive heat flow and nonlinear geothermal gradients in marine sediments—observations from Ocean Drilling Program boreholes, *Geo-Mar. Lett.*, 1–9, doi:10.1007/s00367-015-0425-3.

Thatcher, K. E., G. K. Westbrook, S. Sarkar, and T. A. Minshull (2013), Methane release from warming-induced hydrate dissociation in the West Svalbard continental margin: Timing, rates, and geological controls, *J. Geophys. Res. Solid Earth*, *118*, 22–38, doi:10.1029/2012JB009605.

Tréhu, A. M., P. B. Flemings, N. L. Bangs, J. Chevallier, J. E. Johnson, C.-S. Liu, X. Liu, M. Riedel, and M. E. Torres (2004), Feeding methane vents and gas hydrate deposits at south Hydrate Ridge, *Geophys. Res. Lett.*, *31*, L23310, doi:10.1029/2004GL021286.

Van Genuchten, M. T. (1980), A closed-form equation for predicting the hydraulic conductivity of unsaturated soils, *Soil Sci. Soc. Am. J.*, *44*(5), 892–898.

Waite, W. F., L. A. Stern, S. H. Kirby, W. J. Winters, and D. H. Mason (2007), Simultaneous determination of thermal conductivity, thermal diffusivity and specific heat in sI methane hydrate, *Geophys. J. Int.*, *169*(2), 767–774, doi:10.1111/j.1365-246X.2007.03382.x.

Wallmann, K., E. Pinero, E. Burwicz, M. Haeckel, C. Hensen, A. Dale, and L. Ruepke (2012), The global inventory of methane hydrate in marine sediments: A theoretical approach, *Energies*, *5*(7), 2449–2498, doi:10.3390/en5072449.

Warzinski, R. P., I. K. Gamwo, E. J. Rosenbaum, E. M. Myshakin, H. Jiang, K. D. Jordan, N. J. English, and D. W. Shaw (2008), Thermal properties of methane hydrate by experiment and modeling and impacts upon technology, in Proceeding of the 6th international conference on gas hydrates, Vancouver.

Weaver, J. S., and J. M. Stewart (1982), In situ hydrates under the Beaufort shelf, in Proceedings, Canadian Permafrost Conference, 4th, 1981: Ottawa, National Research Council of Canada, 312–319.

Westbrook, G. K., et al. (2009), Escape of methane gas from the seabed along the West Spitsbergen continental margin, *Geophys. Res. Lett.*, *36*, L15608, doi:10.1029/2009GL039191.

Xu, W., R. P. Lowell, and E. T. Peltzer (2001), Effect of seafloor temperature and pressure variations on methane flux from a gas hydrate layer: Comparison between current and late Paleocene climate conditions, *J. Geophys. Res.*, *106*(B11), 26,413–26,423, doi:10.1029/2001JB000420.